Geophysical Prospecting, 2007, **55**, 1–12

Detection of preferential infiltration pathways in sinkholes using joint inversion of self-potential and EM-34 conductivity data

A. Jardani[1,2], A. Revil[3*], F. Santos[4], C. Fauchard[5] and J.P. Dupont[1]

[1]*CNRS University of Rouen, UMR 6143 Morphodynamique Continentale et Côtière, Département de Géologie, Rouen, France,* [2]*Bureau d'Etudes ALISE, 76160 Saint Jacques-sur-Darnétal, France,* [3]*CNRS-CEREGE, UMR 6635, Université Paul Cézanne, Aix-Marseille III, Aix-en-Provence, France,* [4]*Departamento de Fisica and Centro de Geofısica da Universidade de Lisboa, 1749-016 Lisboa, Portugal and* [5]*Laboratoire Régional des Ponts et Chaussées de Rouen, 76121 Grand-Quevilly, France*

Received July 2006, revision accepted March 2007

ABSTRACT

The percolation of water in the ground is responsible for measurable electric potentials called self-potentials. These potentials are influenced by the distribution of the electrical conductivity of the ground. Because sinkholes are associated both with self-potential and electrical conductivity anomalies, a joint inversion of EM-34 conductivity and self-potential data is proposed as a way of delineating the location of these features. Self-potential and EM conductivity data were obtained at a test site in Normandy (France) where sinkholes and crypto-sinkholes are present over a karstic area in a chalk substratum overlain by clay-with-flint and loess covers. The presence of sinkholes and crypto-sinkholes is associated with negative self-potential anomalies with respect to a reference electrode located outside the area where the sinkholes are clustered. The sinkholes also have a conductivity signature identified by the EM-34 conductivity data. We used the simulated-annealing method, which is a global optimization technique, to invert jointly EM-34 conductivity and self-potential data. Self-potential and electrical conductivity provide clear complementary information to determine the interface between the loess and clay-with-flint formations. The sinkholes and crypto-sinkholes are marked by depressions in this interface, focusing the groundwater flow towards the aquifer contained in the chalk substratum.

1 INTRODUCTION

In Normandy (France), some of the sinkholes penetrating into the chalk substratum are masked by a loess and clay-with-flint sedimentary cover (Laignel *et al*. 2004). Hydrogeological data indicate that the karst has a binary flow, consisting of a slow recharge, associated with infiltration of water through the matrix of the sedimentary cover, and rapid events, associated with strong rains and the fast percolation of water through the network of sinkholes. Locating sinkholes in the chalk substratum is important for several reasons. The sinkholes are responsible for the vulnerability of the chalk aquifer to agricultural water, which contains pesticides and nitrates. In addition, the development of sinkholes over time is associated with the risk of collapse of the ground (e.g. Nichol 1998).

Some of the sinkholes are clearly visible on the ground surface. They appear as more or less pronounced circular depressions. The sinkholes are clustered along fractures in the chalk bedrock (e.g. Nichol 1998; Salvatia and Sasowskyb 2002), which channel shallow groundwater drainage pathways. However, some of the sinkholes are not visible on the ground because they are not mature enough to create a depression in the ground surface. Indeed, the sinkholes start as microcaves formed by dissolution-enlargement of some initial fractures in the chalk, which also correspond to depressions of the clay-with-flint/loess interface. As the microcaves enlarge, the overlying sediments are channelled down into the chalk,

* E-mail: revil@cerege.fr

creating a void within the clay-with-flint formation. At this stage, these sinkholes are called crypto-sinkholes, and non-intrusive geophysical methods are required to map their positions. As time passes, more and more clay-with-flint and loess are lost down the drains and the voids grow. This creates a continuous subsidence of the ground or the collapse of the voids, resulting in the formation of a sinkhole visible on the ground surface.

Several geophysical methods have been tested in the past to detect sinkholes. They include conductivity mapping with the EM-31 and EM-34 methods (Ahmed and Carpenter 2003), gravimetry (Closson *et al*. 2003), ground-penetrating radar, and electrical resistivity tomography using multi-array electrodes (van Schoor 2002; Zhou, Beck and Adams 2002). Surface geophysical data can also be combined with downhole measurements to locate sinkholes more accurately (Wedekind *et al*. 2005). Ground-penetrating radar cannot be used if the overburden is conductive (e.g. in the presence of a clay-rich cover, as in the present study). DC-electrical resistivity and gravimetry cannot be used to survey a large region, due to the time required for the acquisition of the data.

The geophysical methods listed above are not sensitive to the direction of groundwater flow. Recently, several works have focused on the use of the self-potential method to survey sinkholes and karst (e.g. Erchul and Slifer 1987; Wanfang, Beck and Stephenson 1999; Wedekind *et al*. 2005). Self-potential signals are generated when water flows through a porous material and drags the excess of electric charge contained in the porewater into the so-called electrical double layer (e.g. Leroy and Revil 2004). Previous authors (Zablocki 1978; Jackson and Kauahikaua 1987; Aubert and Atangana 1996) have shown that self-potential signals can be related to the percolation of water into the vadose zone. Jardani, Dupont and Revil (2006) used a finite-element code to demonstrate that the self-potential method can be used qualitatively to detect the position of crypto-sinkholes and sinkholes because they form vertical preferential pathways for the flow of the groundwater, which are characterized by negative self-potential anomalies. The self-potential method is the only geophysical method that is sensitive to groundwater flow. It is also an inexpensive and efficient method for surveying large fields quickly. However, the interpretation of self-potential is also dependent on the conductivity distribution of the medium. Self-potential is therefore not a stand-alone method. Electromagnetic methods can also be used to survey very large areas quickly, and because electrical conductivity is sensitive to the water and clay contents of the formation, it provides information, in addition to self-potential data, to detect sinkholes.

The goal of the present study is to test the effectiveness of combining self-potential and EM-34 conductivity data for locating sinkholes and crypto-sinkholes. In addition, we performed surveys at two different periods of the hydrological cycle to show how these methods are sensitive to hydrological parameters (water content and groundwater flux). In Section 2, we describe the test site located in Normandy (France), where sinkholes are present in a chalk formation. In Section 3, we interpret two self-potential surveys, performed in spring and summer 2005, over a test site. We quantify the self-potential survey made in spring to determine the thickness of the loess layer, which corresponds to the unsaturated zone. In Section 4, we invert the apparent electrical conductivity data obtained with the EM-34 apparatus, and we discuss the variations of the data in the spring and in the summer. In Section 5, we present a joint inversion of EM-34 conductivity and self-potential data to determine the geometry of the loess/clay-with-flint interface, using a simulated-annealing algorithm.

2 DESCRIPTION OF THE TEST SITE

The test site investigated in this paper is located in Normandy (France) in the Upper Cretaceous chalk karst of the Western Paris basin (Fig. 1). In this region of extensive agricultural

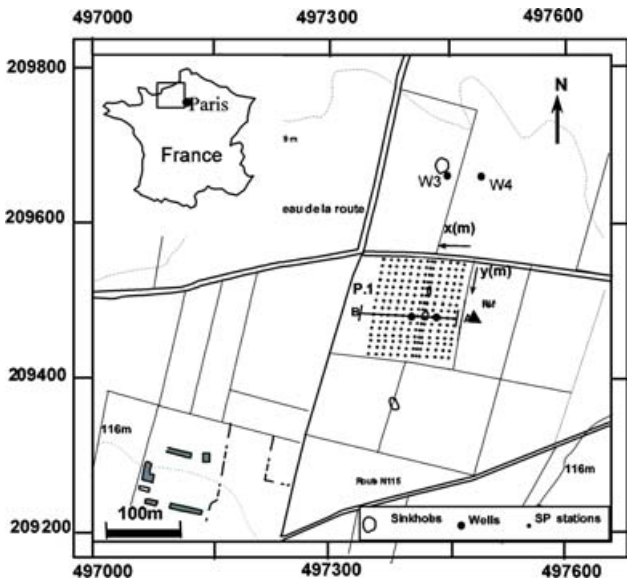

Figure 1 Location of the test site in Normandy (NW France). At this test site, the sinkholes are all aligned along a N–S trend. Four boreholes were drilled over the test site.

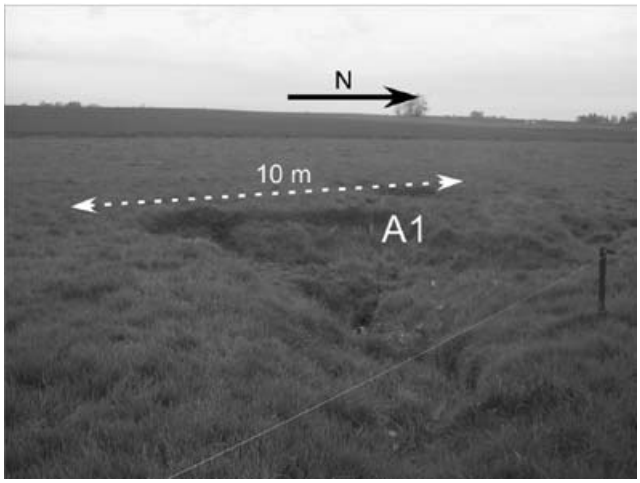

Figure 2 Picture of sinkhole A1. Its diameter is 10 m and the depth of the depression is approximately of 2 m.

areas, sinkholes and crypto-sinkholes are frequently clustered in a thick chalk substratum. The cover of this substratum is composed of Pliocene clay-with-flint and loess materials resulting from the alteration of the chalk substratum (Laignel *et al*. 2004). The thickness of this cover ranges from a few metres to 10 metres outside sinkholes. It can reach ~15 m over some sinkholes. The permeability of the upper units is relatively low (~10^{-5} m s^{-1} for the loess cover to 10^{-10} m s^{-1} for the clay-with-flint cover, see Jardani *et al*. 2006). Due to the contrast in permeability between the loess and the clay-with-flint covers, a shallow perched aquifer exists above the clay-with-flint formation in spring. Water flow is predominantly lateral in this upper flow system until a sinkhole is encountered. Sinkholes act as local vertical pathways through the clay, connecting the shallow upper flow system to the main aquifer located in the chalk formation at a depth of about 30 m. Five boreholes drilled at the test site demonstrate the existence of this shallow aquifer above the clay-with-flint cover (Jardani *et al*. 2006). The sinkholes are marked by approximately circular depressions in the ground (see Fig. 2). The sinkholes that are not visible at the ground surface are called crypto-sinkholes.

3 SELF POTENTIAL SURVEY

3.1 Background

The percolation of water through a porous material generates an electric field of electrokinetic nature called the streaming potential. In fact, the surfaces of all the minerals in contact with water become charged. To compensate for this excess or deficiency of electric charges, a net charge accumulation of opposite sign develops in the porewater. This phenomenon is called the electric double layer (e.g. Leroy and Revil 2004). The drag of the charge density contained in the porewater is therefore responsible for polarization of the medium (e.g. Revil *et al*. 1999; Revil, Leroy and Titov 2005, and references therein). Several methods have been described in the past to relate self-potential signals to the geometry of groundwater flow pathways (e.g. Fournier 1989; Aubert and Atangana 1996; Revil *et al*. 2003). The self-potential method is a passive geophysical method that measures the electric potential between two non-polarizing electrodes placed on the ground surface of the earth. One of these electrodes is placed at a fixed (reference) position in the field (outside the area where it is suspected that the sinkholes are located), while the other is used to scan the electric potential at the ground surface at different locations (see Fig. 3). In the present study, non-polarizing electrodes consisted of a bare copper cylinder immersed in a supersaturated copper-sulphate solution in a porous ceramic cup. The self-potentials between the reference station and the scanning electrode are measured with a calibrated Metrix MX-20 voltmeter with a sensitivity of 0.1 mV and an internal impedance of 100 MΩ (calibration was checked with a set of resistances with F. Perrier). The distance between two measurement stations was 10 m and 5 m in the outer and central parts of the investigated areas, respectively. A total of 225 measurements were performed over a surface area of 15 400 m^2. Jardani *et al*. (2006) showed that the standard deviation of the self-potential measurements, at this specific site, was 1 mV. This means a very high signal-to-noise ratio and a high reproducibility of the measurements. Using finite-element modelling, Jardani *et al*. (2006) showed that the sinkholes are associated with negative self-potential anomalies of a few tens of millivolts.

3.2 Interpretation

Spring data

The self-potential map realized in spring 2005 shows negative anomalies (Fig. 3a). Spring is the rainy season in Normandy. During spring 2005, the total rainfall was 400 mm. As modelled by Jardani *et al*. (2006), the percolation of water into the sinkholes in spring is responsible for a negative self-potential signature with anomalies of −30 mV (see the self-potential anomalies A1 and A2 in Fig. 3a). The position of these self-potential anomalies provides a footprint signature of their location. The density of self-potential stations used in this study is insufficient to allow the shape of the sinkholes to be

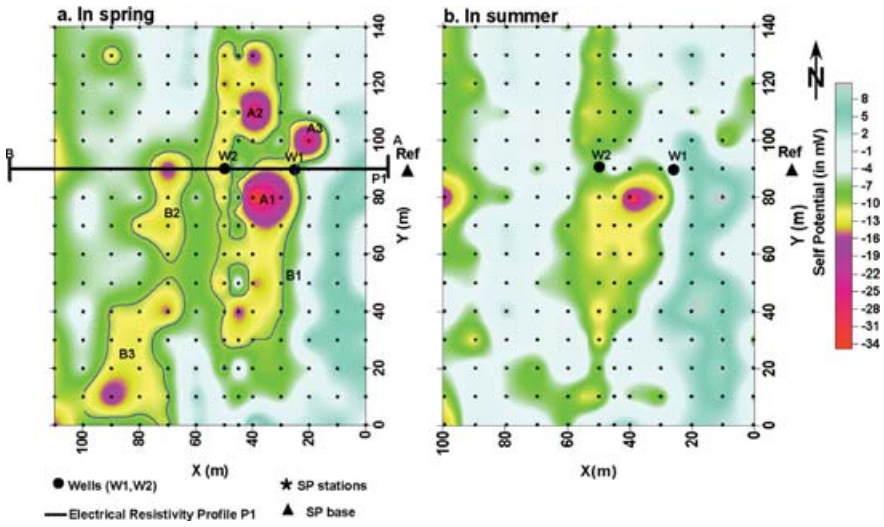

Figure 3 Self-potential map of the test site. The small stars correspond to the stations where the self-potential was measured (Ref indicates the position of the self-potential reference station). The self-potential data were obtained (a) in spring and (b) in summer. W1 and W2 are two boreholes. AB is a multi-electrode resistivity profile P1. Anomalies A1 and A2 are two sinkholes visible on the ground surface. They are located on the depression of the clay-with-flint/loess interface (see Fig. 5). Anomaly A3 is either a potential crypto-sinkhole that is located outside this depression or a possible artefact as shown later (Fig. 11).

determined precisely. Wider anomalies (B1, B2 and B3) correspond to topographic lows of the clay-with-flint/loess interface. All these anomalies are clustered along a N–S trend at the test site (Fig. 3a). This trend is also the trend along which the visible sinkholes are clustered (see Fig. 1).

The anomaly A3 could be a crypto-sinkhole. The areas near anomalies B2 and B3 (amplitude −20 mV) are topographic lows of the clay/loess interface (see Jardani *et al.* 2006). We interpret them also as potential crypto-sinkholes. In our opinion, these interpretations are linked, i.e. the topographic lows of the interface are related to zones of enhanced flow that would lead to enhanced dissolution of the chalk.

Jardani *et al.* (2006) used the finite-element code Comsol Multiphysics 3.2 to show that the percolation of water through the vadose zone is responsible for its electrical polarization. In our case, the vadose (unsaturated) zone corresponds to the loess layer because drill-holes show that the clay-with-flint formation always remains water-saturated throughout the year. Based on the assumption first proposed by Jackson and Kauahkana (1987), i.e. self-potential negative anomalies are proportional to the thickness of the vadose zone, Aubert and Atangana (1996) proposed using the following fomula to determine the bottom of the vadose zone (Aubert and Atangana 1996; Aubert, Dana and Gourgaud 2000):

$$H(x, y) = h(x, y) - e_0 - \varphi(x, y)/c, \quad (1)$$

where $H(x, y)$ is the altitude (with respect to a datum) of the bottom of the vadose zone below the measurement station P(x, y), $h(x, y)$ is the altitude of the ground surface at station P(x, y), e_0 is the thickness of the vadose zone below the reference self-potential station (where, by definition, the self-potential signal is equal to zero), φ is the measured self-potential signal at station P(x, y), and c is an apparent voltage coupling coefficient usually expressed in mV/m. As explained above, the vadose zone corresponds to the loess layer. It follows that the bottom of the vadose zone also corresponds to the interface between the clay-with-flint cover and the loess formation. We know the position of this interface from two boreholes. It is also very well marked on the two DC resistivity surveys shown in Figs 4 and 5. Jardani *et al.* (2006), showed that by taking $c = -5.7$ mV/m and $e_0 = 2$ m, we can reconstruct the position of the bottom of the vadose zone (called the SPS surface in the terminology of Aubert and co-workers). The result is shown in Figs 6 and 7.

Summer data

Summer 2005 was a very dry period in France. In summer, the self-potential map indicates fewer anomalies in comparison with the map made with the spring data (see Fig. 3a, b). However, the summer self-potential map shows the position of the main sinkholes at the test site (such as sinkhole A1).

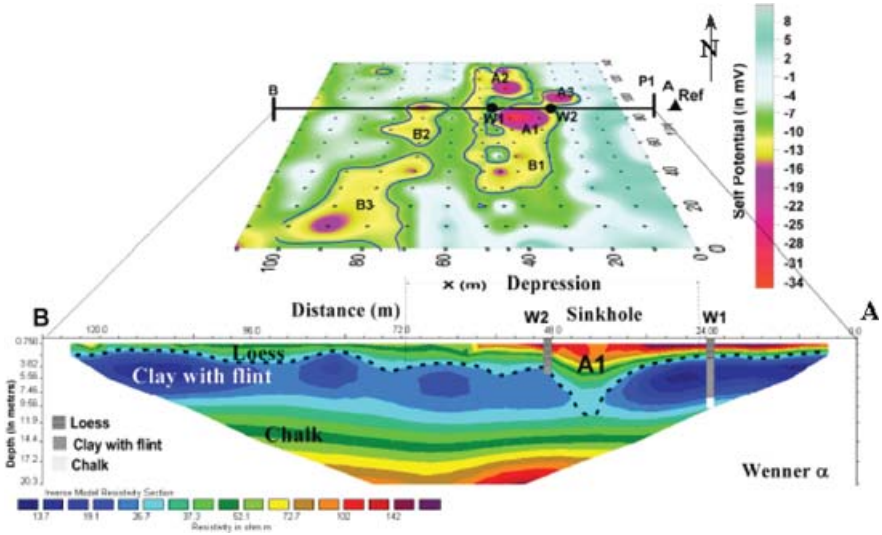

Figure 4 Comparison between the self-potential map and the inverted electrical resistivity section. Electrical resistivity tomography along profile P1 (electrode spacing 3 m, Wenner-α array). The electrical resistivity tomography is shown at the fourth iteration (RMS error: 1.39%). The Wenner-α array is not sensitive to variations of the electrical conductivity in the chalk formation below the sinkhole.

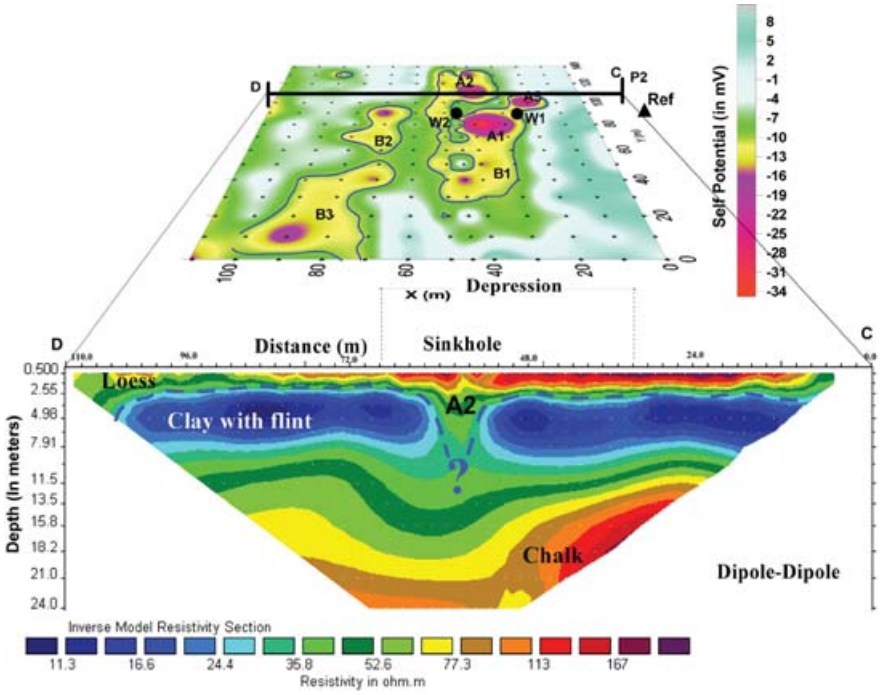

Figure 5 Electrical resistivity tomography along profile P2 (electrode spacing 4 m, dipole–dipole array).The electrical resistivity tomography is shown at the 4th iteration (RMS error: 4.1%). Note the conductive root in the chalk formation below the sinkhole. There is also a sinkhole at the beginning of the profile, just outside the investigated area.

Consequently, water still percolates through this sinkhole but this infiltration comes from the slow percolation of water from the clay-with-flint formation and not from the percolation of water from the shallow aquifer lying just above the clay-with-flint/loess interface. The lower permeability of the clay-with-flint layer is compensated by the greater surface of discharge offered for the infiltration. Indeed, in summer, the boreholes installed over the studied area show no free water above the

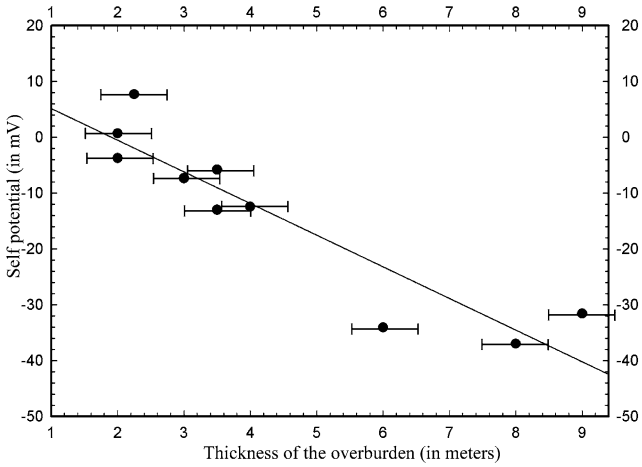

Figure 6 Correlation between the self-potential signals $\varphi(P)$ and the thickness of the loess layer $e(x, y)$ ($R = 0.83$) (data from profile P1). The data for the thickness of the vadose zone are taken from the DC-resistivity survey. The apparent voltage coupling coefficient c, determined from the slope of this linear trend, is equal to -5.7 mV/m.

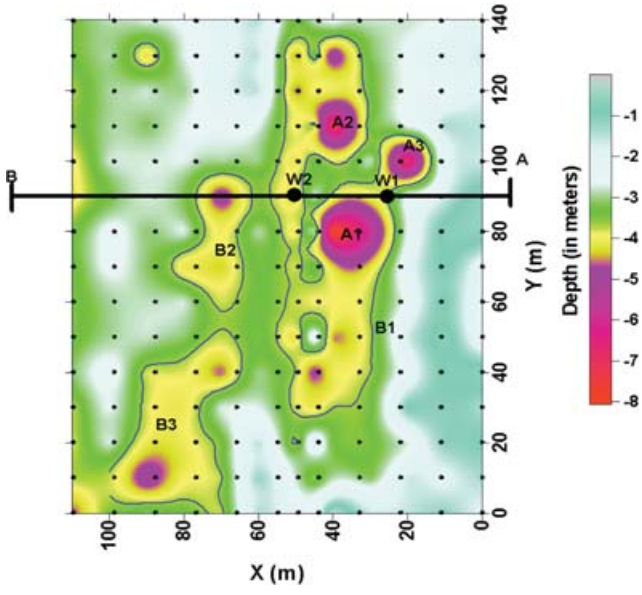

Figure 7 Determination of the depth of the SPS surface (expressed in m) using the self-potential data measured in spring. This interface corresponds to the interface between the clay-with-flint cover and the loess formation. The apparent coupling coefficient used to derive the depth of this interface is determined from the correlation between the self-potential anomalies and the thickness of the loess layer determined from the electrical resistivity tomographies.

clay-with-flint formation. In addition, the monitoring of the self-potential signals in summer shows positive signals during the day (not shown here) that are probably due to evaporation of water in the vadose zone.

4 ELECTROMAGNETIC RESISTIVITY SURVEYS

4.1 EM conductivity data

Electromagnetic (EM) methods (e.g. with the EM-31 and the EM-34 tools) are useful and simple methods for determining the electrical conductivity distribution of shallow sedimentary formations. These methods have already been used successfully in karstic areas (see Ahmed and Carpenter 2003). However, the drawback of these methods is that they do not always possess a strong vertical resolution. The EM-34 equipment was described by McNeill (1980). The basic instrument consists of two coils. The first one is the transmitter, which is energized with an alternating current at a specific frequency; the second one, located at a short distance from the former, is the receiver. The variable magnetic field created by the transmitter (the primary field) induces electric currents in the ground. These currents generate a secondary magnetic field, which is detected, together with the primary field, by the receiver coil. The investigation depth depends on the frequency of the energizing field, on the electrical resistivity of the ground, and also on the intercoil spacing and the coil configuration (vertical dipole or horizontal dipole modes).

We performed two EM-34 resistivity surveys in 2005. In spring 2005, we used the vertical-loop mode to collect the data with two different depths of investigation and an intercoil separation distance of 10 m and 20 m, respectively. The conductivity map obtained with the spacing of 10 m is shown in Fig. 8(a). Another survey was performed during summer 2005 using a vertical spacing of 10 m (Fig. 8c). In Fig. 8(a, b), we compare the conductivity data obtained in spring with the coil spacings of 10 and 20 m, respectively.

4.2 Interpretation

Spring data

In the spring, there was a high water content in the shallow formations in comparison with the situation in the summer. To check the values of the water content in the vicinity of a sinkhole and far from it, we drilled two boreholes, W3 and W4 (see location in Fig. 1) to obtain gravimetric water content versus depth curves at these boreholes. The gravimetric water content was measured by weighting the extracted samples before and after oven drying. These data show that the water content of the vadose zone seems to be higher above a sinkhole than at a far distance from it. We have no explanation for this observation, which is, at first glance,

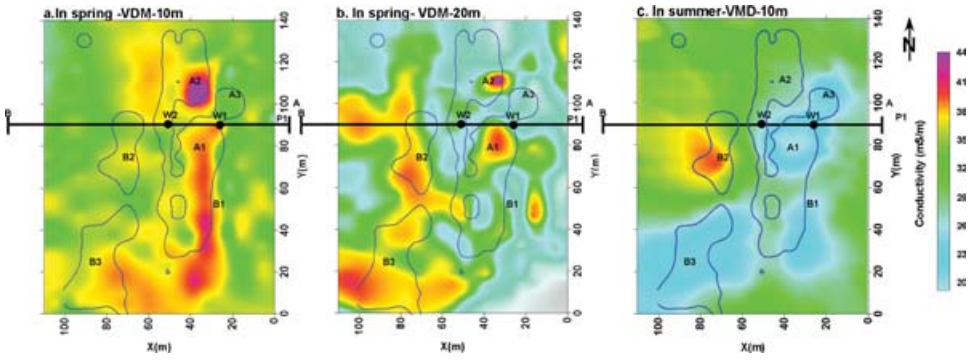

Figure 8 (a) Conductivity map in spring (EM-34, intercoil spacing 10 m, vertical dipole mode). (b) Electrical conductivity map in spring (EM-34, intercoil spacing 20 m, vertical dipole mode). At this depth, conductive areas show alteration of the chalk formation. (c) Conductivity map in summer (EM-34, intercoil spacing 10 m, vertical dipole mode). The closed lines represent the boundaries of the self-potential negative anomalies measured in spring (see Fig. 4a). In spring, there is a very high conductivity structure with a N–S trend. This area corresponds to a depression in the interface between the clay-with-flint and loess formations. High conductivity is consistent with high water content inside this formation, which channels groundwater. Note that the conductivity of the shallow formations is much lower in summer by comparison with spring. This is consistent with the fact that the water content is lower is summer than in spring.

surprising. Indeed, the sinkholes are responsible for drainage of the perched loess aquifer during the spring. The gradient needed to produce this flow toward the sinkhole would cause an increasing hydraulic head (i.e. increasing water-table elevation) moving away from the sinkhole. As the level of the water table rises, so would the capillary fringe and, therefore, the average water content would increase. This is in contrast to the observation made at wells W3 and W4. Could the difference in water content between well W3 and well W4 simply be the result of local heterogeneity? We cannot provide an answer to this question. However, the conductivity map obtained in the spring (Fig. 8a) indicates a conductive area with a N–S trend. This area could correspond to an area of high water content because of the high apparent electrical conductivity (37 to 40 mS/m) of this anomaly. Figure 9 shows that the water content, aznd hence the electrical conductivity, is higher above sinkholes than outside their area. Indeed, various authors (e.g. Kachanoski, Gregorjch and Van Wesenbeeck 1988) have established a quantitative relationship between the variation of the electrical conductivity and the variation of the water content for various types of sediments. For loess, Rhoades, Raats and Prather (1976) showed that a volumetric change of 2 to 5% of the water content can be responsible for a variation of 1 to 2 mS/m of the electrical conductivity. Therefore, we interpret this conductive anomaly as associated with a set of sinkholes and crypto-sinkholes in this area.

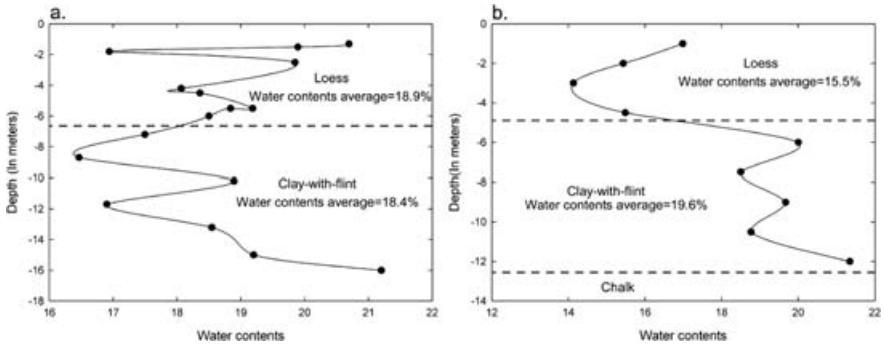

Figure 9 Water content versus depth for samples taken into boreholes W3 and W4 (see their location on Fig. 1, data obtained in May, 2005). (a) Data in borehole W3. (b) Data in borehole W4. Note that in borehole W3, located in the vicinity of a sinkhole, the water content in the vadose zone is higher than that in borehole W4, located further from the sinkhole. In borehole W4, we observe a greater difference in the water content between the loess and the clay-with-flint formations in comparison with the data of borehole W3, where the water content is roughly the same for the two formations.

Summer data

Summer 2005 was very dry in Normandy and therefore the water content in the shallow formations was very low in comparison with the situation in the spring. This is confirmed by the low electrical conductivity values (10 to 20 mS/m) (Fig. 8c). During the summer, the boreholes show that there are no shallow aquifers above the clay-with-flint formation, confirming the dryness of the loess cover during this period.

4.3 Inversion of the EM data

To invert the EM-34 conductivity data, we use a smooth inversion technique (Constable, Parker and Constable 1987; Sasaki 1989). A 1D laterally constrained approach was described in detail by Monteiro Santos, Matias and Gonçalves (2001) and Monteiro Santos (2004). This approach yields the distribution of the electrical conductivity of the ground at depths of 2.5 m, 10 m and 15 m (see Fig. 10a, b, c). At 2.5 m, the water content of the loess formation is high, probably because of the high value of the electrical conductivity. This is confirmed by the observations made in two wells. The depth of 10 m corresponds to the position of the interface between the clay-with-flint and chalk formations. The conductivity map indicates two types of highly conductive anomaly. One of them is associated with the roots of the sinkholes and the crypto-sinkholes. Because of the presence of clay particles in this area of high drainage (that originates from the collapse of the clay formation), the formation appears more conductive. An alternative explanation for the increased electrical conductivity (and permeability) could be the presence of secondary porosity generated during the disorderly collapse of the sediments into the sinkhole.

Figure 10(c) shows the electrical conductivity distribution at a depth of 15 m. We observe the conductive root of sinkhole A1. The resistive substratum is associated with the unaltered chalk formation while the more conductive areas correspond to the altered chalk formation.

5 SP-EM JOINT INVERSION

Inversion of electromagnetic data is a non-linear problem that can be solved by applying local optimization algorithms like constrained linearization techniques (e.g. Tikhonov and Arsenin 1977; Constable *et al*. 1987). It is widely recognized that the solutions produced by these methods depend on the initial values of the model parameters and the value of the regularization parameter. In recent years, the interest in the application of global optimization techniques (e.g. genetic algorithm, controlled random search, simulated annealing, etc.) to geophysical problems has gained in popularity. This is because (i) with these methods, there is no need to determine the Jacobian matrix (i.e. calculate derivatives) and (ii) it is more likely to reach a global minimum of the objective function rather than a local minimum (Kirkpatrick, Gelatt and Vecchi 1983; Pessel and Gibert 2003).

We use here the simulated-annealing algorithm to jointly invert self-potential and conductivity data. A detailed description of the simulated-annealing algorithm can be found in Kirkpatrick *et al*. (1983). The method was developed by analogy with the process of physical annealing in thermodynamics: the undetermined parameters of the geophysical model are analogous to the particles of the physical system and the objective function of the inverse problem is analogous to its global energy. Similarly to the thermodynamic annealing process, which is controlled by the initial temperature and cooling

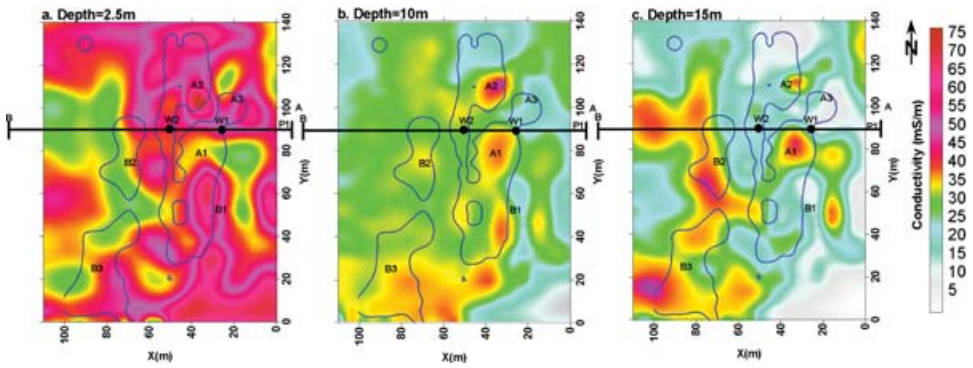

Figure 10 Results of the inversion of the EM-34 data. We show the distribution of the electrical conductivity at different depths: (a) 2.5 m; (b) 10 m; (c) 15 m.

process, the solution of the inverse problem is also controlled by a positive parameter T called the temperature. The model parameters are changed (randomly) during the inversion process. The acceptability of a change is based on the Metropolis algorithm (Metropolis *et al*. 1953). According to this algorithm, perturbations of the parameters that lead to a decrease in the objective function are unconditionally accepted. When an increase in the objective function is checked, the acceptance of the change in the parameters depends on the value of the function ψ (which represents an acceptance probability) that is compared with a randomly generated number χ between 0 and 1. The changes in the model are accepted if $\psi > \chi$, and are rejected otherwise. The function ψ is defined as

$$\psi = \exp(-\Delta E/T), \tag{2}$$

where ΔE represents the objective function variation. For high T values, virtually all changes are accepted. The Metropolis algorithm is iterated over a sequence of models at a constant T value. This renders the solution independent of the initial model and allows the algorithm to escape from local minima. It is expected that the accepted models will concentrate in the vicinity of the absolute minimum while T decreases. It is important to decrease the value of the parameter T slowly for convergence efficiency of the simulated-annealing algorithm, allowing a representative sampling of the full parameter space (Monteiro Santos *et al*. 2006).

In order to apply the simulated-annealing algorithm to the joint inversion of SP and EM conductivity data, the subsurface is divided into two domains separated by an irregular boundary. The medium of each layer is subdivided into hexahedral cells. Each cell is characterized by its electrical conductivity, top and bottom interface depths and an apparent voltage coupling coefficient c defined in mV/m.

Self-potential forward calculations were performed based on equation (1), while cumulative functions were used in EM forward calculations (McNeil 1980; Monteiro Santos *et al*. 2001). At low induction numbers, the magnetic coupling between ground current loops induced by the primary field is negligible. In this case, it is possible to construct a function of depth $S(z)$, that describes the relative contribution to the secondary magnetic field, measured at the receiver, of the homogeneous material within a thin horizontal layer at a depth z (McNeill 1980). In a layered-earth model, the relative contribution to the secondary magnetic field from all material below a depth z can be expressed by the cumulative function $R_{\mathrm{H,V}}$ (for horizontal or vertical coplanar transmitter/receiver dipole configurations) as defined by McNeill (1980):

$$R = \int_z^\infty S(z)\ \mathrm{d}z. \tag{3}$$

The expressions for the functions $R_{\mathrm{V,H}}(Z)$ are (McNeill 1980)

$$R_{\mathrm{V}}(Z) = \frac{1}{\sqrt{4Z^2+1}}, \tag{4a}$$

$$R_{\mathrm{H}}(Z) = \sqrt{4Z^2+1} - 2Z, \tag{4b}$$

where Z is the depth of the ith layer divided by the intercoil spacing. Taking into account these definitions, the response of an N-layered earth is calculated adding the contribution from each layer independently, weighted accordingly to its conductivity and depth.

In the scope of this work, the use of the cumulative response to calculate the model response at each measuring point means that we do not consider the electromagnetic interaction between constituent blocks of the model. However, the inversion algorithm constrains each block parameter to be dependent on its neighbours to a certain degree. According to equations (1) and (4), the self-potential and the EM data are both determined by the vadose zone thickness. Therefore, the depth of the SPS surface will be the common parameter for the SP and EM joint inversion.

We need to define a global objective function Q, based on the L_1-norm, and involving a weighted sum of four objective functions. These objective functions are the objective function of the self-potential data (E_{SP}), the objective function of the electromagnetic data (E_{EM}), as well as the objective functions corresponding to the depth of the SPS surface (E_{SPS}), and the cells conductivity roughness (E_{Con}). The global objective function Q is defined as

$$Q = \varepsilon_1 E_{\mathrm{SP}} + \varepsilon_2 E_{\mathrm{EM}} + \varepsilon_3 E_{\mathrm{SPS}} + \varepsilon_4 E_{\mathrm{Con}}, \tag{5}$$

where ε_1, ε_2, ε_3 and ε_4 are weights. The values of these weights depend on the relative importance of the self-potential data and the electromagnetic data, the roughness of the SPS surface and the conductivity of the cells, respectively. They also depend on the data error and *a priori* variance of the model parameters. The objective functions E_{SP} and E_{EM} are defined by

$$E = \frac{2\sum_{i=1}^{N} \left| y_i^{\mathrm{obs}} - y_i^{\mathrm{cal}} \right|}{\sum_{i=1}^{N} \left| y_i^{\mathrm{obs}} - y_i^{\mathrm{cal}} \right| + \sum_{i=1}^{N} \left| y_i^{\mathrm{obs}} + y_i^{\mathrm{cal}} \right|}. \tag{6}$$

The observed and calculated data values are denoted by superscripts obs and calc, respectively and y denotes SP potential

or EM apparent conductivity. N is the number of SP or EM measured values. E_{Con} and E_{SPS} roughness are defined as

$$E = \frac{1}{N}\sum E_{ij}, \tag{7}$$

$$E_{ij} = E_{i-1,j-1} + E_{i-1,j+1} + E_{i+1,j-1} + E_{i+1,j+1} - 4E_{i,j}, \tag{8}$$

where E_{ij} represents the conductivity of the (i,j)th cell or the depth of the SPS surface that limits the (i,j)th cell.

We now investigate the sensitivity and equivalence problems in our formulation. From equation (1), the SP signal is proportional to the product of the thickness of the first layer (corresponding to the vadose zone) and the apparent coupling coefficient. This means that possible equivalent models can be obtained as long as this product is kept constant. On the other hand, the derivative of equation (1),

$$\frac{\partial e}{\partial c} = -\frac{\varphi}{c^2}, \tag{9}$$

(where e is the thickness of the vadose zone) shows that the sensitivity of the model to the thickness of the vadose layer decreases when the coupling coefficient has high values ($c >$ 4.5 mV/m). An investigation of the dependence of the EM apparent conductivity on the depth of the interface between the two media, through the derivatives $(\partial\sigma_{\mathrm{a}}/\partial Z)_{\mathrm{V,H}}$, shows that the data loses sensitivity to the depth when it increases. From these results and from the fact that our models are a rough approximation of the reality, some variability in the model parameters is expected. The best model of the joint inversions of the depth of the clay-with-flint/loess interface is shown in Fig. 11. This result was obtained with $\varepsilon_1 = \varepsilon_2 = \varepsilon_3 = \varepsilon_4 = 1$, which means that we give the same confidence to all four objective functions. The global misfit between the field data and the model response is 25%. Several other models, using different weighting values, have been obtained. However, they showed greater misfit and more variability in the SPS results.

The two main sinkholes, A2 and A1, are clearly visible in Fig. 11, plus an additional crypto-sinkhole that we name A4 and two diffuse depressions, B2 and B3. The sinkhole A3 was probably an artefact and is not visible on the joint inversion of the EM-34 and self-potential data. The roots of the sinkholes are visible to a depth of approximately 7 m. The present results encourage us to investigate more cases in hydrogeophysics and to explore new combinations of geophysical techniques for quantitatively treating the geometry of the percolation pathways of water in such environments.

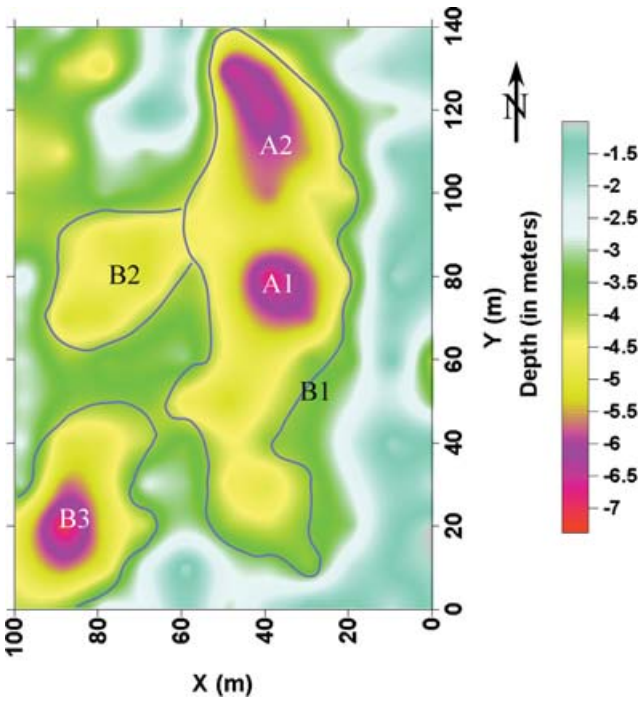

Figure 11 Determination of the depth of the interface between the loess (partially saturated) and clay-with-flint (water-saturated) formations using the joint inversion of the self-potential and EM-34 data. In spring, a shallow aquifer is located above the clay-with-flint cover. The water of the aquifer above the clay-with-flint cover is channelled to the karstic conduits that connect the shallow aquifer to the deep aquifer located at a depth of roughly 30 m in the chalk substratum. The anomaly A3 has disappeared.

6 CONCLUSIONS

The self-potential and electromagnetic (EM-34) methods provide complementary information to reconstruct the geometry of the subsurface and to locate sinkholes and crypto-sinkholes in the chalk substratum of Normandy (France). The self-potential method is the only geophysical method that is sensitive to the flow of groundwater while the inversion of the EM-data provides the distribution of electrical conductivity, which is sensitive to the water and clay contents of the shallow cover. We have proposed a joint inversion of self-potential and electromagnetic EM to reconstruct the 2D shape of the clay-with-flint/loess interface. We used the simulated-annealing method as a global optimization technique to solve this problem. Sinkholes and crypto-sinkholes correspond to marked depressions of this interface. The groundwater is channelled above the clay-with-flint formation until it percolates through the sinkholes and the crypto-sinkholes to a deeper aquifer located in the chalk formation. Future work will include induced

polarization as a source of additional information to determine the permeability structure of these formations.

ACKNOWLEDGEMENTS

We thank the University of Rouen, the CNRS, and IRIS Instrument for their support. We would also like to thank C. Gioa, T. Leboulonger, M. Simon and the editor and two anonymous referees for their helpful reviews of our manuscript. This work is supported by ANR Project ERINOH and ANR-ECCO-PNRH Project POLARIS.

REFERENCES

Ahmed S. and Carpenter P.J. 2003. Geophysical response of filled sinkholes, soil pipes and associated bedrock fractures in thin mantled karst, east central Illinois. *Environmental Geology* **44**, 705–716.

Aubert M. and Atangana Q.Y. 1996. Self-potential method in hydrogeological exploration of volcanic areas. *Ground Water* **34**(6), 1010–1016.

Aubert M., Dana I.I.N. and Gourgaud A. 2000. Internal structure of the Merapi summit from self-potential measurements. *Journal of Volcanology and Geothermal Research* **100**, 337–343.

Closson D., Karaki N.A., Hussein M.J., Al-Fugha H., Ozer A. and Mubarak A. 2003. Subsidence et effondrements le long du littoral jordanien de la mer Morte : apport de la gravimétrie et de l'interférométrie radar différentielle. *C. R. Geosciences* 335, 869–879.

Constable S.C., Parker R.L. and Constable C.G. 1987. Occam's inversion: a practical algorithm for generating smooth models from electromagnetic sounding data. *Geophysics* **52**, 289–300.

Erchul R.A. and Slifer D.W. 1987. The use of spontaneous potential in the detection of groundwater flow patterns and flow rate in karst areas. *Proceedings of 2nd Conference on Karst Hydrogeology*, Orlando, USA, pp. 217–226.

Fournier C. 1989. Spontaneous potentials and resistivity surveys applied to hydrogeology in a volcanic area: case history of the Chaîne des Puys (Puy-de-Dôme, France). *Geophysical Prospecting* **37**, 647–668.

Jackson D.B. and Kauahikaua J. 1987. Regional SP anomalies at Kilauea. Volcanism in Hawaii. *USGS Prof.* paper 1350, **40**, 947–959.

Jardani A., Dupont J.P. and Revil A. 2006. Self-potential signals associated with preferential groundwater flow pathways in sinkholes. *Journal of Geophysical Research*, **37**, B09204. doi:10.1029/2005JB004231

Kachanoski R.G., Gregorjch E.G. and Van Wesenbeeck I.J. 1988. Estimating spatial variations of soil water content using noncontacting electromagnetic induction methods. *Canadian Journal of Soil Science* **68**, 715–722.

Kirkpatrick S., Gelatt C. Jr. and Vecchi M. 1983. Optimization by simulated annealing. *Science* **220**, 671–680.

Laignel B., Dupuis E., Rodet J., Lacroix M. and Massei N. 2004. An example of sedimentary filling in the chalk karst of the Western Paris Basin: characterization, origins, and hydrosedimentary behaviour. *Z. F. Géomorphologie* **48**(2), 219–243.

Leroy P. and Revil A. 2004. A triple layer model of the surface electrochemical properties of clay minerals. *Journal of Colloid and Interface Science* **270**(2), 371–380.

McNeill J.D. 1980. *Electromagnetic terrain conductivity measurement at low induction numbers*. Geonics Limited, Technical Note TN-6.

Metropolis N., Rosenbluth A., Rosenbluth M., Teller A. and Teller E. 1953. Equation of state calculations by fast computing machines. Journal of Chemical Physics **21**(6), 1087–1092.

Monteiro Santos F.A. 2004. 1D laterally constrained inversion of EM34 profiling data. *Journal of Applied Geophysics* **56**, 123–134.

Monteiro Santos F.A., Matias H. and Gonçalves R. 2001. The use of EM34 surveys in cave detection. *European Journal of Environmental and Engineering Geophysics* **6**, 153–166.

Monteiro Santos F.A., Sultan S.A., Represas P. and El Sorady A.L. 2006. Joint inversion of gravity and geoelectrical data for groundwater and structural investigation: application to the northwestern part of Sinai, Egypt. *Geophysical Journal International* doi:10.1111/j.1365–246X.2006.02923.x

Nichol D. 1998. Sinkholes at Glan Llyn on the A55 North Wales Coast Road, UK. *Engineering Geology* **50**, 101–109.

Pessel M. and Gibert D. 2003. Multiscale electrical impedance tomography. *Journal of Geophysical Research* **108**(B1), doi: 10.1029/2001JB000233.

Revil A., Leroy P. and Titov K. 2005. Characterization of transport properties of argillaceous sediments. Application to the Callovo-Oxfordian Argillite. *Journal of Geophysical Research* **110**, B06202, doi: 10.1029/2004JB003442.

Revil A., Naudet V., Nouzaret J. and Pessel M. 2003. Principles of electrography applied to self-potential electrokinetic sources and hydrogeological applications. *Water Resources Research* **39**(5), 1114, doi: 10.1029/2001WR000916.

Revil A., Schwaeger H., Cathles L.M. and Manhardt P. 1999. Streaming potential in porous media. 2. Theory and application to geothermal systems. *Journal of Geophysical Research* **104**(B9), 20 033–20 048.

Rhoades J.D., Raats P.A.C. and Prather R.J. 1976. Effects of liquid-phase electrical conductivity, water content and surface conductivity on bulk soil electrical conductivity. *Soil Science Society of America Journal* **40**, 651–655.

Salvatia R. and Sasowskyb I. 2002. Development of collapse sinkholes in areas of groundwater discharge. *Journal of Hydrology* **264**, 1–11.

Sasaki Y. 1989. Two-dimensional joint inversion of magnetotelluric and dipole-dipole resistivity data. *Geophysics* **54**, 254–262.

van Schoor M. 2002. Detection of sinkholes using 2D electrical resistivity imaging. *Journal of Applied Geophysics* **50**, 393–399.

Tikhonov A.N., and Arsenin V.Ya. 1986. *Methods for Solving Ill-Posed Problems*. Nauka, Moscow (in Russian).

Wanfang Z., Beck B.F. and Stephenson J.B. 1999. Investigation of groundwater flow in karst areas using component separation of natural potential measurements. *Environmental Geology* **37**(1–2), 19–25.

Wedekind J.E., Osten M.A., Kitt E. and Herridge B. 2005. Combining surface and downhole geophysical methods to identify karst conditions in North-central Iowa. *Geotechnical Special Publication* **144**, 616–625.

Zablocki C.J. 1978. Streaming potentials resulting from the descent of meteoric water. A possible source mechanism for Kilauean self-potential anomalies. *Geothermal Research Council, Transactions* **2**(2), 747–748.

Zhou W., Beck B.F. and Adams A.L. 2002. Effective electrode array in mapping karst hazards in electrical resistivity tomography. *Environmental Geology* **42**(8), 922–928.